Spin–phonon coupling in monoclinic BiCrO 3

B. Araújo, A. M Arévalo-López, C. Santos, J. Attfield, C. Paschoal, A. Ayala

Journal of Applied Physics

Spin–phonon coupling in monoclinic $BiCrO_3$

Cite as: J. Appl. Phys. **127**, 114102 (2020); https://doi.org/10.1063/1.5143347
Submitted: 22 December 2019 . Accepted: 22 February 2020 . Published Online: 16 March 2020

B. S. Araújo, A. M. Arévalo-López, C. C. Santos, J. P. Attfield, C. W. A. Paschoal, and A. P. Ayala

Journal of Applied Physics ARTICLE scitation.org/journal/jap

Spin–phonon coupling in monoclinic $BiCrO_3$

Cite as: J. Appl. Phys. **127**, 114102 (2020); doi: 10.1063/1.5143347
Submitted: 22 December 2019 · Accepted: 22 February 2020 ·
Published Online: 16 March 2020

View Online Export Citation CrossMark

B. S. Araújo,[1,2] A. M. Arévalo-López,[2,3] C. C. Santos,[4] J. P. Attfield,[2] C. W. A. Paschoal,[1] and A. P. Ayala[1,a)]

AFFILIATIONS

[1]Physics Department, Federal University of Ceará, Campus do Pici, 60455-760 Fortaleza, CE, Brazil
[2]Centre for Science at Extreme Conditions (CSEC) and School of Chemistry, The University of Edinburgh, Peter Guthrie Tait Road, Edinburgh EH9 3FD, United Kingdom
[3]University of Lille, CNRS, Centrale Lille, ENSCL, University Artois, UMR 8181—UCCS—Unité de Catalyse et Chimie du Solide, F-59000 Lille, France
[4]Physics Department, CCET, Federal University of Maranhão, PO Box 65085-580, São Luís, MA, Brazil

[a)]**Author to whom correspondence should be addressed:** ayala@fisica.ufc.br

ABSTRACT

Monoclinic $BiCrO_3$, synthesized at high pressure and high temperature, presents interesting properties with anomalies of magnetic origin observed around 110 and 80 K, which are associated, respectively, with the rise of a G-type antiferromagnetic structure and the spin reorientation along one of the monoclinic axes. In this study, we report a strong spin–phonon coupling in monoclinic $BiCrO_3$ observed by Raman spectroscopy. The renormalization of the phonon energy confirms the coupling with the magnetic orderings. Interestingly, some phonons exhibit this effect at the rising temperature of the G-type antiferromagnetic ordering, whereas others are sensitive to the second magnetic event. A renormalization model based on the mean-field theory, previously applied to other perovskite compounds, was used to analyze the spin–phonon coupling showing different behaviors associated with each magnetic phase.

I. INTRODUCTION

Chromates with perovskite structure $ACrO_3$ have been investigated intensively in the last few years due to their interesting properties and applications. While rare-earth-based compounds exhibit intriguing magnetic properties[1–3] and multiferroic behavior at low temperatures,[4] Bi-based chromites are interesting because they are lead-free ferroelectric and multiferroic materials.[5–7]

Particularly, $BiCrO_3$ (BCO) obtained by a high-pressure and high-temperature method crystallizes in a monoclinic structure with the *C2/c* space group. Such a structure transforms into an orthorhombic *Pnma* structure ($GdFeO_3$-type phase) around 420 K.[8] However, powder x-ray diffraction measurements confirmed that the *Pnma* structure is still present at low temperatures in the BCO compound. Thus, it was assumed that a *C2/c–Pnma* phase coexistence is a stable state.[9,10] This feature directly drives the BCO magnetic properties since the long-range G-type antiferromagnetic (AFM) ordering around $T_N = 110$ K is associated with the *C2/c* phase, whereas two anomalies at 40 K and 165 K are due to the *Pnma* one.[10] Belik and co-workers reported the first observation of the magnetic event around 40 K for $BiCrO_3$[11] through a slight anomaly in the ZFC curve for measurements at 100 Oe and a strong frequency-dependent anomaly in the imaginary part of the magnetic susceptibility. Later, Belik and Takayama-Muromachi[9] associated this event with the coexistence of the Pnma structure in the monoclinic phase. These conclusions were reinforced by Belik[10] in a review related to polar and nonpolar phases of $BiMO_3$ compounds. Also, a magnetic anomaly was reported being characterized by a large increase in the magnetization curve in the interval between 80 K and 60 K. This event is due to a spin reorientation, where the spin moments form a 50° angle with the monoclinic b direction,[12] preserving the G-type antiferromagnetic structure.[10] Two interesting features in the BCO magnetic behavior are the frequency-dependent magnetic properties below 40 K, which still needs further explanation and the two-step AFM transition at 80 K and 110 K.[10,12]

Concerning the BCO electric properties, there are still many open questions. Dielectric properties of bulk BCO were investigated at high temperatures by Niitaka *et al.*[8] describing an anomaly in the dielectric constant around 420 K. However, first-principles density functional calculations predicted an antiferroelectric behavior associated with the structural distortions at high temperatures.[13]

In thin films, the contradictions remain. For example, Murakami *et al.*[5] reported the growth of room temperature ferroelectric BCO by pulsed laser deposition (PLD) in $LaAlO_3$ (001), $SrTiO_3$ (001), and $NdGaO_3$ (110) substrates. Meanwhile, Kin *et al.*[14] observed that BCO thin films obtained by PLD on $SrTiO_3$ (001) with the $SrRuO_3$ bottom electrode exhibit antiferroelectricity with an electric field induced ferroelectric phase, as confirmed by double hysteretic behaviors in the electric field dependence of the dielectric constant and polarization.

The Raman spectrum of polycrystalline bulk and thin films of BCO was first reported by Himcinschi *et al.*[15] In this study, the authors confirmed the monoclinic to orthorhombic phase transition at 400 K described by Niitaka *et al.*[8] However, the authors did not report any spectral anomaly on the interval between 120 and 87 K, which could be related to the reported magnetic events.

Despite the contradictions on the dielectric properties, the possible coupling between electric and magnetic ordering suggests that the magnetic order can also couple with the lattice. In this way, Raman scattering spectroscopy is a powerful technique due to its sensibility to detect magnetic orderings through the coupling with lattice phonons, which was verified in several perovskite compounds.[8,16,17] Thus, the temperature dependence of the Raman-active phonons below room temperature can help elucidate the BCO magnetic and electric behavior and their coupling.

II. EXPERIMENTAL DETAILS

Polycrystalline samples of BCO were synthesized by a solid-state reaction under high pressure and high temperature (HPHT). Stoichiometric amounts of Bi_2O_3 (99.9%) and Cr_2O_3 (99.9%) were ground and sealed into platinum capsules and treated at 1273 K under 6 GPa during 60 min in a Walker type multi-anvil press. After the reaction, the system was quenched to room temperature (RT), and the pressure was slowly released. The resultant samples were dark-green dense pellets and were characterized by x-ray powder diffraction (XRPD) on a BRUKER D8 diffractometer (Cu $K\alpha_1$ radiation 1.5406 Å). The values of lattice parameters and sub-phase portions were refined by the Rietveld method using the GSAS software package.[18]

Magnetization data were obtained on a commercial magnetometer (Quantum Design Magnetic Properties Measurement System). Temperature dependence of the magnetic susceptibility in zero-field cooled (ZFC) and field cooled (FC) conditions were recorded in the 2–300 K temperature range with a 0.5 T (5 kOe) applied field.

Raman spectroscopy measurements were performed in a Jobin-Yvon T64000 Triple Spectrometer configured in a backscattered geometry. The 633 nm line of a HeNe gas laser operating at 2 mW, focused on the sample by a long-working distance objective (20×, 20.5 mm), was used to excite the signal that was collected in an N_2-cooled CCD system. Temperature-dependent Raman measurements from 10 up to 300 K were carried out by using a closed-cycle He cryostat in which a Lakeshore temperature controller model 330S stabilized the temperature with a precision of 0.1 K. The Raman spectra were deconvoluted with Lorentzian functions using Fityk software (version 0.9.8).[19]

III. RESULTS AND DISCUSSION

The powder x-ray diffraction measurement of the synthesized dark-green polycrystalline pellets of $BiCrO_3$ is shown in Fig. 1.

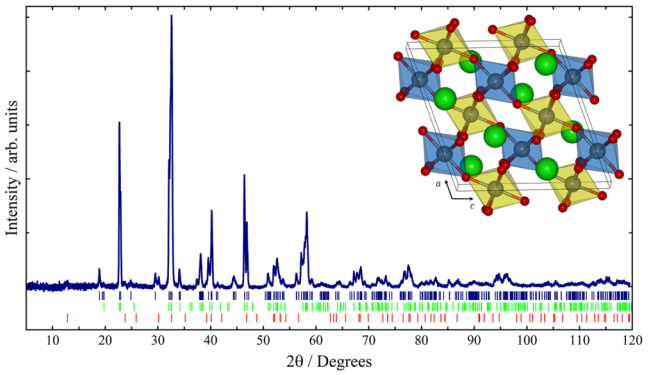

FIG. 1. XRPD pattern obtained from as-synthesized BCO samples. Dark blue bars indicate the peaks of the standard monoclinic *C2/c* phase[20] (ICSD number 160455), green bars indicate the orthorhombic phase[9] (ICSD number 160454), and red bars indicate the Bi_2CO_3 (ICSD number 36245). The inset shows the perovskite BCO monoclinic *C2/c* structure where the octahedra are shown with different colors to indicate the opposite spin moments of G-type antiferromagnetic ordering.

The pattern was analyzed using the Rietveld method and presented a monoclinic perovskite-type structure belonging to the *C2/c* space group. The refined cell parameters are *a*: 9.4685(3) Å, *b*: 5.4811(2) Å, *c*: 9.5856(3) Å, and *β*: 108.574(2)°, in good agreement with those reported by other authors.[8,11,20] It was proposed that an orthorhombic BCO phase could coexist with the monoclinic one at and below room temperature. Thus, following the approach proposed by Belik and Takayama-Muromachi,[9] the orthorhombic phase of BCO was added to the Rietveld refinement. This treatment reveals the presence of a *Pnma* sub-phase with an approximate concentration of 9% of the weight fraction (w.f.), with lattice parameters *a*: 5.5649(6) Å, *b*: 7.7313(8) Å, and *c*: 5.4845(7) Å, in accord with those reported by Belik and Takayama-Muromachi[9] Also, the BCO diffraction pattern showed the presence of $Bi_2(CO_3)O_2$, with a proportional amount of approximately 2% w.f., as it is usual in the HPHT synthesis of BCO.[12,21]

As a standard perovskite, the BCO crystalline structure exhibits a corner-shared CrO_6 octahedra lattice, with Bi ions located in the free space between such octahedra (the inset of Fig. 1). In this configuration, the octahedra are tilted according to the Glazer tilting system $a^-b^-b^-$ related to the ideal cubic perovskite.[22]

Figure 2 shows the zero-field cooled (ZFC) and field cooled (FC) magnetic susceptibilities of BCO between 3 and 300 K. As expected from previous works,[11,12,20] the magnetic susceptibility curve shows the appearance of magnetic contributions around 110 K attributed to the rise of a G-type antiferromagnetic structure. At this temperature, a sudden rise in susceptibility can also be noted, which has been associated with a weak ferromagnetic ordering.[8,10–12] Also, a large increase in the magnetic susceptibility intensity is noted around 80 K, which is related to the spin reorientation along the *b* axis.[12] Based on previous reports,[9] two additional anomalies on magnetic susceptibility, ascribed to the presence of the orthorhombic phase, were expected around 40 and 165 K. A subtle change in the first derivative of magnetic susceptibility was observed around 40 K (the inset of Fig. 2), related to the fraction of

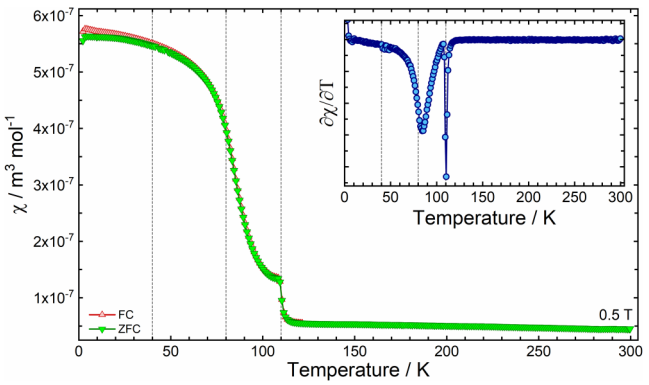

FIG. 2. Magnetic susceptibility curves obtained from $BiCrO_3$ samples. The red and green triangles are the ZFC and FC results, respectively. The inset panel shows the first derivate of zero-field cooled magnetic susceptibility. Dashed lines indicate the temperatures of reported BCO magnetic events.[9,11]

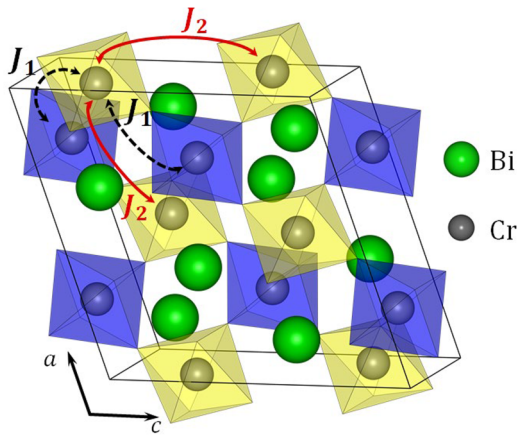

FIG. 3. Schematic representation of exchange paths in the unit cell of BCO (oxygen atoms placed at the octahedra vertices).

Pnma found in the XRPD analysis. Thus, the magnetic properties of our samples are mainly determined by the antiferromagnetic G-type ordering at 110 K and the spin alignment around 80 K. These characteristics are in good agreement with the magnetic behavior reported in the literature.

Anderson[23] suggested that not only the nearest neighbor (NN) interactions but also the next nearest neighbor (NNN) interactions have an essential role in understanding complex magnetic orderings in antiferromagnetic materials, mainly when they present a high θ_{CW}/T_N ratio. For BCO, each Cr ion is surrounded by one set of two Nearest Neighbor (NN) Cr ions, whose distances are 3.87 and 3.94 Å, and one set of two Cr ions (5.47 and 5.57 Å) associated with the Next Nearest Neighbor (NNN). The fitted effective magnetic moment (μ_{eff}) and the Weiss constant (θ_{CW}) have values around $4\mu_B$ and -360 K,[8,11] respectively, giving a $|\theta_{CW}/\ T_N|$ ratio approximately of 3.27. This ratio value highlights the complex character of the BCO magnetic structure especially when compared with the one of 3.09 observed in $YCrO_3$,[24] which also presents a weak ferromagnetic phase in a complex competition with the main antiferromagnetic phase. Others indicative of strong NN and NNN interactions are the estimated values of their respective exchange constants J_1 and J_2 (illustrated in Fig. 3). By means of the molecular field theory, those interaction constants can be related to the Curie–Weiss constant (θ_{CW}) and the Neel Temperature (T_N), following the approach proposed by Tsushima *et al.*,[25]

$$J_1 = \frac{K_B}{8s(s+1)} \cdot (\theta_{CW} - T_N),$$
$$J_2 = \frac{1}{2} \cdot \frac{K_B}{8s(s+1)} \cdot (\theta_{CW} + T_N). \quad (1)$$

The values of the exchange constants were estimated by using the experimental θ_{CW} and T_N, giving $J_1 = -10.89\,\mathrm{cm}^{-1}$ and $J_2 = -2.90\,\mathrm{cm}^{-1}$. The values presented for BCO are lower than those reported for $SmCrO_3$ ($J_1 = -13.54\,\mathrm{cm}^{-1}$ and $J_2 = -4.64\,\mathrm{cm}^{-1}$)[26] but still are comparable with those of $YCrO_3$ ($J_1 = -13.48$ and $J_2 = -3.45\,\mathrm{cm}^{-1}$),[24] indicating that the J_2 NNN interactions are not negligible in this system.

Figure 4(a) shows the unpolarized BCO Raman spectrum measured at room temperature. According to the group theory analysis, based on the site occupation of the $C2/c$ monoclinic structure, 27 Raman-active modes are expected at the Γ point of the Brillouin zone.[27] These modes can be decomposed on the irreducible representations of the C_{2h} point group as $13\,A_g \oplus 14\,B_g$. In Fig. 4(a), 13 of the 27 Raman-active predicted modes are observed. This number of modes is also in good accordance with the Raman results reported by Himcinschi *et al.*[15]

The assignment of the observed Raman modes based on those of the ABO_3 perovskite family already reported in the literature[28–31] is shown in Table I. The external modes are located below 180 cm^{-1}, while those with higher wavenumbers are related to CrO_6 octahedral motions. The modes around 184 and 362 cm^{-1} have A_g symmetry and are related to in-phase y rotations and out-of-phase x rotations, respectively. Those observed at 289 and 340 cm^{-1} have A_g and B_g symmetries, respectively, being related to the basal octahedra oxygen motion along the x and z axis. The octahedra bending and out-of-phase bending have A_g symmetry and are observed at 402 and 417 cm^{-1}, respectively. Finally, the mode located at 538 cm^{-1} has a B_g symmetry, and it is due to the anti-stretching octahedra vibration. It is notable that in this study, the A_g modes are more intense than B_g ones, and this finding is in agreement with those reported for the monoclinic phase of $BiMnO_3$[32] and polarized measurements reported by Talkenberger *et al.*[33] and Himcinschi *et al.*[15] for the monoclinic BCO phase.

In the temperature-dependent study of BCO Raman spectra, we were able to monitor the behavior of six A_g and two B_g internal modes with mixed symmetries under cooling from 300 K to 10 K. Figure 4(b) exhibits the temperature-dependent Raman spectra obtained for BCO. Since this compound does not present any structural phase transition in the investigated temperature range, we cannot note any remarkable change in the Raman spectra in terms of additional or suppressed bands. The overall signature of

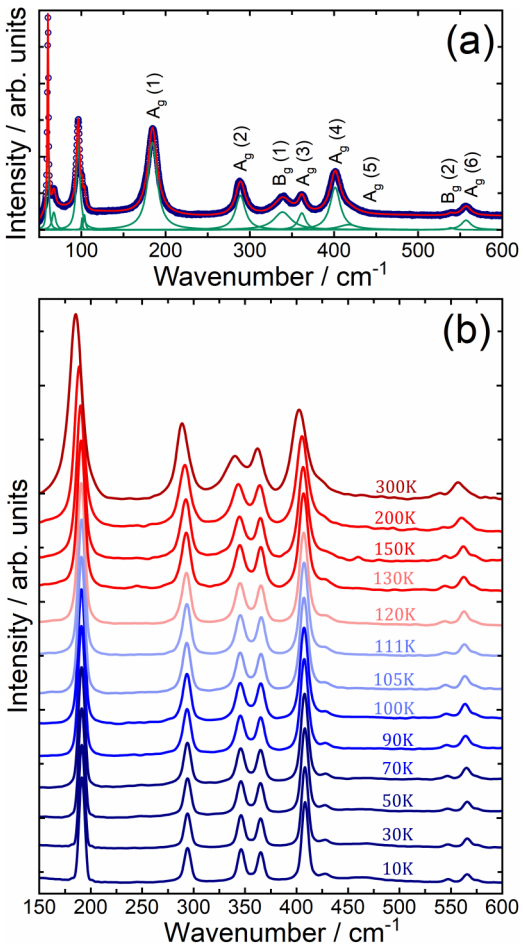

FIG. 4. (a) Room-temperature Raman spectrum of BCO. Open blue circles show the experimental data fitted with individual Lorentzian profiles. The solid red line indicates the best fit for the experimental data. (b) Temperature-dependent Raman spectra of BCO.

the Raman spectra is maintained in the investigated temperature range, and only the usual high-frequency shift and mode sharpening were observed, which can be understood by considering the lattice contraction and reduction of thermal vibrations.

TABLE I. Band position assignments of the observed Raman modes in BCO.

Wavenumber (cm^{-1})	Symmetry	Main atomic motions
185	$A_g(1)$	BO_6 in-phase y rotations
289	$A_g(2)$	O_1(x), A(−x)
340	$B_g(1)$	O_1(−z), A(z)
362	$A_g(3)$	BO_6 out-of-phase x rotations
402	$A_g(4)$	BO_6 bending
417	$A_g(5)$	BO_6 out-of-phase bending
538	$B_g(2)$	O_2, O_1 antistretching
555	$A_g(6)$	…

Usually, in the absence of structural changes, the temperature-dependent behavior of a phonon mode of the frequency ω is mainly governed by the phonon anharmonicity hardening, in which, according to Balkanski's model,[34] the temperature dependence of the phonon frequency is given by

$$\omega(T) = \omega_0 + C\left[1 + \frac{2}{(e^{(\hbar\omega_0/2K_BT)} - 1)}\right] + D\left[1 + \frac{3}{(e^{(\hbar\omega_0/3K_BT)} - 1)} + \frac{3}{(e^{(\hbar\omega_0/3K_BT)} - 1)^2}\right], \quad (2)$$

where ω_0, C, and D are fitting parameters. In this model, the second and third terms on the right side are related to two and three phonon processes, respectively, whereas higher-order phonon interactions were omitted.

Figure 5 shows the temperature dependence of selected phonon energies and their full width at half maximum (FWHM) compared with Balkanski's model. The temperature-dependent positions of such phonons exhibit renormalization from the theoretical model at 110 K for the $A_g(1)$, $A_g(3)$, $B_g(2)$, and $A_g(6)$ modes [Figs. 5(a), 5(c), 5(e), and 5(f), respectively], while the $B_g(1)$ and $A_g(4)$ present this effect below 80 K [Figs. 5(b) and 5(d)]. The stronger renormalizations were observed for $B_g(2)$ and $A_g(6)$ modes, reaching values around 2 cm^{-1}. Notice that $T_N = 110$ K is the temperature of the AFM ordering in BCO, while at 80 K, there is the spin moment realignment around the b axis of the monoclinic structure.[12] Such observations suggest a spin–phonon coupling in BCO at these temperatures. Once the FWHM is related to the phonon lifetime,[35] it is not affected by anomalous thermal lattice variations. Thus, the analysis of the FWHM behavior is an important tool to distinguish between events related to subtle volume changes due to exchange-striction[36] or magnetostriction and phenomena related to coupling effects.[37] In this way, the FWHM for all selected modes also presented subtle renormalizations at 110 and 80 K, indicating the presence of a spin–phonon coupling at these temperatures. The poor FWHM fitting of the $B_g(2)$ [Fig. 5(e)] mode above 110 K is due to the very low intensity of this mode in comparison with the remaining ones.

Besides the events at 110 and 80 K, the Raman results also revealed very subtle changes in the phonon behavior below 40 K. Below this temperature, the position of all analyzed phonons becomes almost constant. This feature is very weak in comparison with those observed for the magnetic events at higher temperatures but still is an indication that the Raman modes in BCO are also sensitive to the magnetic event at 40 K related to the *Pnma* lattice.[9,11]

Srinu Bhadram *et al.*[38] reported the temperature dependence of the Raman spectra of the orthorhombic $RCrO_3$ family. In this study, the authors observed similar spin–phonon coupling effects confirmed through the FWHM analysis of samples where the R^{3+} site is occupied by magnetic ions. Also, Mahana *et al.*[36] recently reported the spin–phonon coupling of $GdCrO_3$ in which the phonon frequencies also presented a mix of hardening and softening effects below T_N, as observed in our BCO study. In both cases, the magnitude of the reported renormalizations was in the order of 1–3 cm^{-1} in good accordance with those observed here.

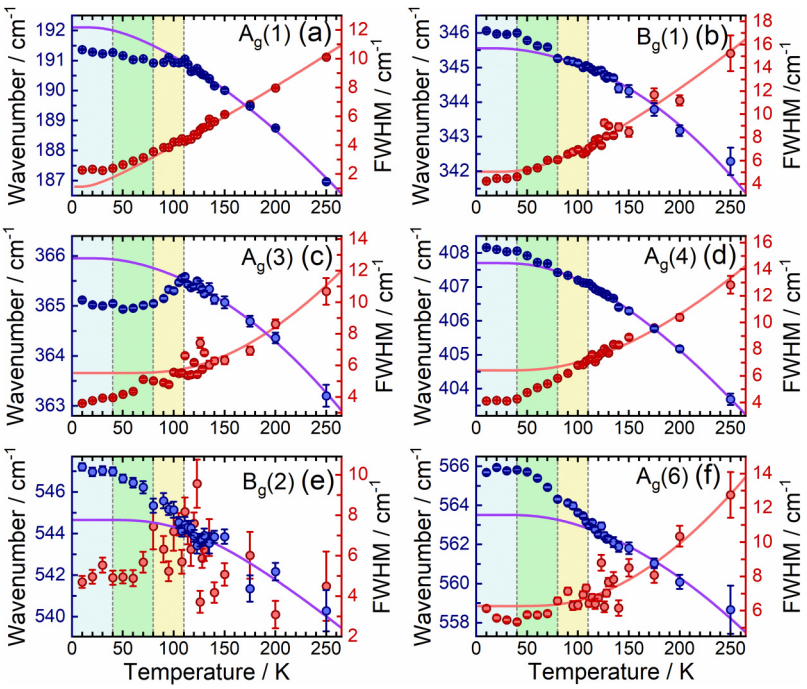

FIG. 5. Panels (a)–(f) Temperature dependence of the phonon energy and full width at half maximum (FWHM) of selected Raman-active modes of BCO. Solid lines are the fit based on Balkanski's model. Dashed lines represent the magnetic events reported in the literature.

The phonon frequency departure from the expected anharmonic behavior of a given vibrational mode as a function of the temperature in a spin ordered phase can be described by taking into account the spin–spin correlation function,[39,40]

$$\Delta\omega(\mathrm{T}) = \lambda\langle\vec{S}_i \cdot \vec{S}_j\rangle = \frac{1}{2\,m\omega}\sum_r \frac{\partial^2 J(r)}{\partial u_r^2}\langle S_i \cdot S_j\rangle, \tag{3}$$

where ω is the renormalized phonon frequency due to a spin–phonon coupling at a fixed temperature, ω_0 is the phonon frequency in the absence of the renormalization effect (dominated only by anharmonic effects), λ is a coupling constant, and $\langle\vec{S}_i \cdot \vec{S}_j\rangle$ denotes a statistical-mechanical average for adjacent spins that belong to sublattices of opposite spins. In a paramagnetic phase, where there are no spin interactions, the $\langle\vec{S}_i \cdot \vec{S}_j\rangle$ term vanishes, while in spin ordered phases, it is expected that the spin–phonon coupling generates additional contributions to the phonon frequencies. In general, besides the magnetic order, λ depends on how the phonon modulates the exchange interaction.[36,41] So far, a general trending on the phonon renormalization due to a spin–phonon coupling has been reported in a large number of compounds. Usually, antiferromagnetic systems present a hardening effect on phonon frequencies,[42,43] whereas ferromagnetic materials show a softening effect.[44,45] Nevertheless, the λ factor has a complex character that depends on the atomic motions involved in the phonon mode, and, for this reason, some compounds seem to be beyond this rule.[24,43,46,47] In the case of BCO, the hardening effect observed for $B_g(1)$, $A_g(4)$, $B_g(2)$, and $A_g(6)$ [Figs. 5(b) and 5(d)–5(f)] are in agreement with the standard trending of AFM materials, while the $A_g(1)$ and $A_g(3)$ [Figs. 5(a) and 5(c)] modes do not follow this tendency, indicating that each phonon mode has a particular and independent λ factor. However, the correlation between magnetic interactions and the phonon modes in the coupling constant is very complex, and the exact form in which those two properties influence the spin–phonon renormalization effect remains unclear.

As mentioned before, a similar mix between hardening and softening frequencies behavior has been reported for $GdCrO_3$,[36] $YCrO_3$,[24] and $BiMnO_3$[48] samples. In the last two cases, the authors attribute this mixed behavior to a competition between weak ferromagnetic and antiferromagnetic phases presented by these materials. To describe the competitive simultaneous ferromagnetic and antiferromagnetic interactions of $CdCr_2S_4$, Wakamura and Arai[49] proposed a theoretical model in which the phonon renormalization (Δω) can be written as

$$\Delta\omega \propto -k_1\langle S_a \cdot S_b\rangle + k_2\langle S_c \cdot S_d\rangle, \tag{4}$$

where k_1 and k_2 are spin-dependent coupling constants depending on the relationship between the exchange integrals and the phonon displacements. In this way, k_1 is associated with the ferromagnetic NN interactions, while k_2 is associated with the antiferromagnetic NNN exchanges.[50] In such a model, the spin correlation function of the nearest and the next nearest neighbors has the same temperature dependence[50] inducing the same correlation functions for $\langle S_a \cdot S_b\rangle$ and $\langle S_c \cdot S_d\rangle$. Therefore, Eq. (4) reduces to Eq. (3) where the complex λ factor arises from the difference between k_1 and k_2, assuming different values for each phonon mode. This model has been used to explain the phonon renormalization due to the spin–phonon coupling in systems such as $BiMnO_3$,[48] which present a ferromagnetic (FM) structure, and $YCrO_3$, which exhibits a G-type anti-ferromagnetic

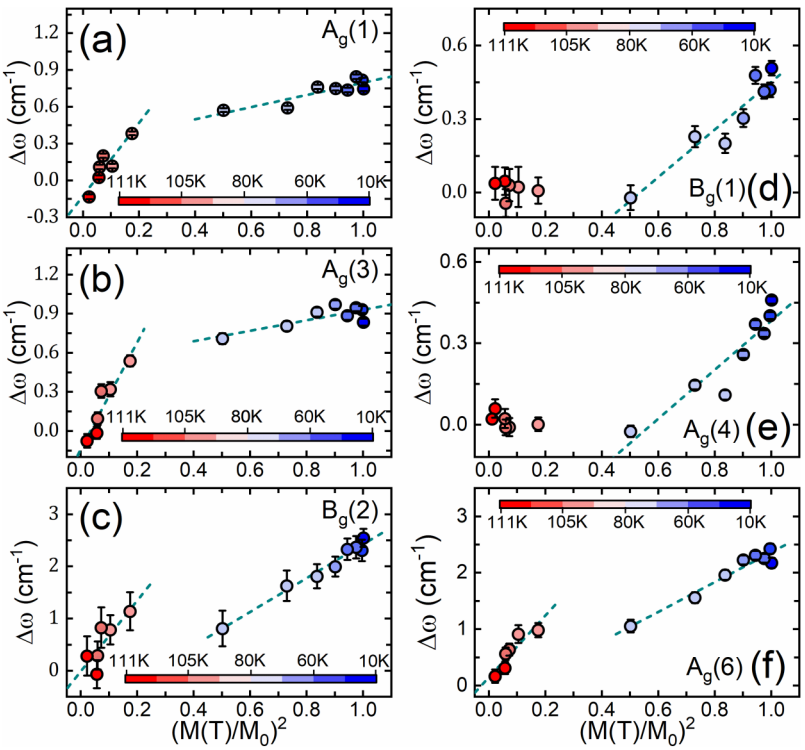

FIG. 6. Panels (a)–(f) Temperature dependence of the departure from the anharmonic frequency behavior of selected phonons as a function of $(M(T)/M_0)^2$, and dark-green dashed lines are the linear fit of data.

(AFM) ordering,[24] and also for different magnetic structures observed in the manganite family $Eu_{1-x}Y_xMnO_3$.[50]

In the case of $BiCrO_3$, a weak ferromagnetic order,[8,10–12] evidenced by the sudden increase in magnetic susceptibility at 110 K (see Fig. 2), is found in coexistence with the G-type antiferromagnetic phase. Then, the approach proposed by Wakamura and Arai[49] could be an explanation for the observed softening effect presented by $A_g(1)$ and $A_g(3)$, while the other modes present a hardening effect.

Based on mean-field approximation, Granado *et al.*[51] proposed a mechanism to describe the phonon renormalization induced by a spin–phonon coupling [Eq. (3)] for perovskite structures; these interactions can be described as

$$\Delta\omega(T) = \omega_0(T) - \omega(T) \propto \left(\frac{M(T)}{M_0}\right)^2, \tag{5}$$

where $M(T)$ is the average magnetization per magnetic ion at temperature T and M_0 is the saturated magnetization. Such a model works well for different perovskites even in a system with antisymmetric phonon renormalizations,[36,47,48] which could be the case of BCO. Figure 6 shows $\Delta\omega$ as a function of $(M(T)/M_0)^2$ as related by Eq. (5). As observed in other perovskite compounds,[35,52–54] these results confirm the existence of a linear correlation between the renormalization on phonon positions and $(M(T)/M_0)^2$, in accordance with the proposed model.

A linear correlation is observed between the square of magnetization and the renormalization in phonon energies for $B_g(1)$ and $A_g(4)$ modes [Figs. 6(d) and 6(e)], below 80 K. This behavior combined with the low renormalization of these phonons [Figs. 5(b) and 5(d), respectively] corroborates the existence of a weak spin–phonon coupling only appearing below the temperature at which the magnetic moments undergo the slight reorientation process. This is an unusual phenomenon, where some phonons are sensitive just to one of the magnetic events and should be associated with the correlation between the symmetry of both the phonons and the exchange integrals.

In the case of $A_g(1)$ and $A_g(3)$ phonons [Figs. 6(a) and 6(b), respectively], the linear behavior appears around 110 K, where $\Delta\omega$ increases linearly with the square of magnetization. However, it can be noted that below 80 K, the linear response slightly changes for both phonons. These findings indicate that besides the spin–phonon coupling starts at 110 K, these phonons are also sensitive to the spin reorientation below 80 K. The same two-step spin–phonon coupling effect is observed for the $B_g(2)$ and $A_g(6)$ phonons [Figs. 6(c) and 6(f), respectively]. In both cases, there is a linear correlation between $\Delta\omega$ and $(M(T)/M_0)^2$ below 110 K and a slope change at 80 K.

IV. CONCLUSIONS

In this paper, we reported the spin–phonon coupling in the monoclinic perovskite $BiCrO_3$. Hardening and softening effects on some phonon frequencies starting at 110 K coincide with the emergence of a G-type antiferromagnetic ordered structure, indicating that a spin–phonon coupling induces the observed phonon renormalization. The coupling behavior is similar to that observed

in octahedra stretching modes in other perovskites, whose phonon renormalization follows a mean-field behavior. Moreover, all spin-coupled phonons have shown to be sensitive to the spin reorientation reported around 80 K, reinforcing the existence of this phenomenon. No anomaly was observed at 165 K, which reveals that if there is a magnetic ordering process at this temperature, it does not couple with the lattice phonons. Finally, the only evidence of the magnetic event at 40 K is a subtle change in the phonon frequency below this temperature, suggesting that the magnetic transition of the orthorhombic sublattice also could drive spin–phonon interactions; however, more detailed investigations need to be performed to confirm this effect.

ACKNOWLEDGMENTS

This study was financed in part by the Brazilian agencies CAPES (Finance Code 001), FUNCAP (No. PRONEX PR2-0101-00006. 01.00/15), and CNPq (Grant No. 427478/2016-2).

REFERENCES

[1]B. Rajeswaran, D. I. Khomskii, A. K. Zvezdin, C. N. R. Rao, and A. Sundaresan, Phys. Rev. B **86**, 214409 (2012).
[2]H. J. Zhao, J. Íñiguez, X. M. Chen, and L. Bellaiche, Phys. Rev. B **93**, 014417 (2016).
[3]H. J. Zhao, L. Bellaiche, X. M. Chen, and J. Íñiguez, Nat. Commun. **8**, 14025 (2017).
[4]J. R. Sahu, C. R. Serrao, N. Ray, U. V. Waghmare, and C. N. R. Rao, J. Mater. Chem. **17**, 42 (2007).
[5]M. Murakami, S. Fujino, S.-H. Lim, C. J. Long, L. G. Salamanca-Riba, M. Wuttig, I. Takeuchi, V. Nagarajan, and A. Varatharajan, Appl. Phys. Lett. **88**, 152902 (2006).
[6]R. V. William, A. Marikani, and D. Madhavan, Ferroelectr. Lett. Sect. **44**, 18 (2017).
[7]J. Ding, X.-B. Kang, L.-W. Wen, H.-D. Li, and J.-M. Zhang, Chin. Phys. Lett. **31**, 107501 (2014).
[8]S. Niitaka, M. Azuma, M. Takano, E. Nishibori, M. Takata, and M. Sakata, Solid State Ionics **172**, 557 (2004).
[9]A. A. Belik and E. Takayama-Muromachi, J. Phys. Conf. Ser. **165**, 012035 (2009).
[10]A. A. Belik, J. Solid State Chem. **195**, 32 (2012).
[11]A. A. Belik, N. Tsujii, H. Suzuki, E. Takayama-muromachi, and Q. B. Center, Inorg. Chem. **46**, 8746 (2007).
[12]C. Darie, C. Goujon, M. Bacia, H. Klein, P. Toulemonde, P. Bordet, and E. Suard, Solid State Sci. **12**, 660 (2010).
[13]N. A. Hill, P. Bättig, and C. Daul, J. Phys. Chem. B **106**, 3383 (2002).
[14]D. H. Kim, H. N. Lee, M. Varela, and H. M. Christen, Appl. Phys. Lett. **89**, 162904 (2006).
[15]C. Himcinschi, I. Vrejoiu, T. Weißbach, K. Vijayanandhini, A. Talkenberger, C. Röder, S. Bahmann, D. R. T. Zahn, A. A. Belik, D. Rafaja, and J. Kortus, J. Appl. Phys. **110**, 073501 (2011).
[16]F. Sugawara, S. Iida, Y. Syono, and S. Akimoto, J. Phys. Soc. Jpn. **20**, 1529 (1965).
[17]F. Sugawara, S. Iiida, Y. Syono, and S. Akimoto, J. Phys. Soc. Jpn. **25**, 1553 (1968).
[18]A. C. Larson, and R. B. Von Dreele, Los Alamos National Laboratory Report LAUR 86, 2004.
[19]M. Wojdyr, J. Appl. Crystallogr. **43**, 1126 (2010).
[20]A. A. Belik, S. Iikubo, K. Kodama, N. Igawa, S. Shamoto, and E. Takayama-Muromachi, Chem. Mater. **20**, 3765 (2008).
[21]C. Goujon, C. Darie, M. Bacia, H. Klein, L. Ortega, and P. Bordet, J. Phys. Conf. Ser. **121**, 022009 (2008).
[22]A. M. Glazer, Acta Crystallogr. Sect. B Struct. Crystallogr. Cryst. Chem. **28**, 3384 (1972).
[23]P. W. Anderson, Phys. Rev. **79**, 705 (1950).
[24]Y. Sharma, S. Sahoo, W. Perez, S. Mukherjee, R. Gupta, A. Garg, R. Chatterjee, and R. S. Katiyar, J. Appl. Phys. **115**, 183907 (2014).
[25]K. Tsushima, K. Aoyagi, and S. Sugano, J. Appl. Phys. **41**, 1238 (1970).
[26]M. Tripathi, R. J. Choudhary, D. M. Phase, T. Chatterji, and H. E. Fischer, Phys. Rev. B **96**, 174421 (2017).
[27]R. P. Bauman, D. L. Rousseau, and S. P. S. Porto, J. Raman Spectrosc. **10**, 253 (1981).
[28]M. C. Weber, J. Kreisel, P. A. Thomas, M. Newton, K. Sardar, and R. I. Walton, Phys. Rev. B **85**, 054303 (2012).
[29]M. N. Iliev, A. P. Litvinchuk, V. G. Hadjiev, Y.-Q. Wang, J. Cmaidalka, R.-L. Meng, Y.-Y. Sun, N. Kolev, and M. V. Abrashev, Phys. Rev. B **74**, 214301 (2006).
[30]M. N. Iliev, M. V. Abrashev, J. Laverdière, S. Jandl, M. M. Gospodinov, Y.-Q. Wang, and Y.-Y. Sun, Phys. Rev. B **73**, 064302 (2006).
[31]N. D. Todorov, M. V. Abrashev, V. G. Ivanov, G. G. Tsutsumanova, V. Marinova, Y.-Q. Wang, and M. N. Iliev, Phys. Rev. B **83**, 224303 (2011).
[32]D. P. Kozlenko, N. T. Dang, S. H. Jabarov, A. A. Belik, S. E. Kichanov, E. V. Lukin, C. Lathe, L. S. Dubrovinsky, V. Y. Kazimirov, M. B. Smirnov, B. N. Savenko, A. I. Mammadov, E. Takayama-Muromachi, and L. H. Khiem, J. Alloys Compd. **585**, 741 (2014).
[33]A. Talkenberger, C. Himcinschi, T. Weißbach, K. Vijayanandhini, I. Vrejoiu, C. Röder, D. Rafaja, and J. Kortus, Thin Solid Films **520**, 4590 (2012).
[34]M. Balkanski, R. R. Wallis, and E. Haro, Phys. Rev. B **28**, 1928 (1983).
[35]H.-M. Eiter, P. Jaschke, R. Hackl, A. Bauer, M. Gangl, and C. Pfleiderer, Phys. Rev. B **90**, 024411 (2014).
[36]S. Mahana, B. Rakshit, R. Basu, S. Dhara, B. Joseph, U. Manju, S. D. Mahanti, and D. Topwal, Phys. Rev. B **96**, 104106 (2017).
[37]A. Nonato, B. S. Araujo, A. P. Ayala, A. P. Maciel, S. Yanez-Vilar, M. Sanchez-Andujar, M. A. Senaris-Rodriguez, and C. W. A. Paschoal, Appl. Phys. Lett. **105**, 222902 (2014).
[38]V. Srinu Bhadram, B. Rajeswaran, A. Sundaresan, and C. Narayana, Europhys. Lett. **101**, 17008 (2013).
[39]W. Baltensperger and J. S. J. Helman, Helv. Phys. Acta **41**, 668 (1968).
[40]D. J. Lockwood and M. G. Cottam, J. Appl. Phys. **64**, 5876 (1988).
[41]J. Laverdière, S. Jandl, A. Mukhin, V. Ivanov, and M. Iliev, Phys. Rev. B **73**, 214301 (2006).
[42]M. N. Iliev, M. V. Abrashev, A. P. Litvinchuk, V. G. Hadjiev, H. Guo, and A. Gupta, Phys. Rev. B **75**, 104118 (2007).
[43]R. X. Silva, H. Reichlova, X. Marti, D. A. B. Barbosa, M. W. Lufaso, B. S. Araujo, A. P. Ayala, and C. W. A. Paschoal, J. Appl. Phys. **114**, 194102 (2013).
[44]M. N. Iliev, H. Guo, and A. Gupta, Appl. Phys. Lett. **90**, 151914 (2007).
[45]R. B. Macedo Filho, A. Pedro Ayala, and C. William de Araujo Paschoal, Appl. Phys. Lett. **102**, 192902 (2013).
[46]E. Aytan, B. Debnath, F. Kargar, Y. Barlas, M. M. Lacerda, J. X. Li, R. K. Lake, J. Shi, and A. A. Balandin, Appl. Phys. Lett. **111**, 252402 (2017).
[47]M. A. Prosnikov, A. N. Smirnov, V. Y. Davydov, R. V. Pisarev, N. A. Lyubochko, and S. N. Barilo, Phys. Rev. B **98**, 104404 (2018).
[48]P. Toulemonde, P. Bordet, P. Bouvier, and J. Kreisel, Phys. Rev. B **89**, 224107 (2014).
[49]K. Wakamura and T. Arai, J. Appl. Phys. **63**, 5824 (1988).
[50]J. A. Moreira, A. Almeida, W. S. Ferreira, J. E. Araújo, A. M. Pereira, M. R. Chaves, J. Kreisel, S. M. F. Vilela, and P. B. Tavares, Phys. Rev. B **81**, 054447 (2010).
[51]E. Granado, A. García, J. A. Sanjurjo, C. Rettori, I. Torriani, F. Prado, R. Sánchez, A. Caneiro, S. B. Oseroff, R. D. Sa, and T. Lamno, Phys. Rev. B **60**, 11879 (1999).
[52]R. B. Macedo Filho, D. A. B. B. Barbosa, H. Reichlova, X. Marti, A. S. De Menezes, A. P. Ayala, C. W. A. A. Paschoal, R. B. M. Filho, and A. S. de Menezes, Mater. Res. Express **2**, 075201 (2015).
[53]R. X. Silva, M. C. Castro Júnior, S. Yáñez-Vilar, M. S. Andújar, J. Mira, M. A. Señarís-Rodríguez, and C. W. A. Paschoal, J. Alloys Compd. **690**, 909 (2017).
[54]R. R. Das, P. N. Lekshmi, S. C. Das, and P. N. Santhosh, J. Alloys Compd. **773**, 770 (2019).